RSC Advances

ROYAL SOCIETY OF CHEMISTRY

www.rsc.org/advances

Cite this: DOI: 10.1039/c0xx00000x

www.rsc.org/xxxxxx

ARTICLE TYPE

Ultra-Flyweight Hydrophobic Poly(m-phenylenediamine) Aerogel with Micro-Spherical Shell Structures as A High-Performance Selectivity Adsorbent for Oil Contamination‡

Xun Song [a†], Siwei Yang [b†*], Lin He [a], Shuai Yan [a], Fang Liao [a*]

Received (in XXX, XXX) Xth XXXXXXXXX 20XX, Accepted Xth XXXXXXXXX 20XX
DOI: 10.1039/b000000x

In this paper, the ultra-flyweight hydrophobic poly(m-phenylenediamine) aerogel (PmPDA) was fabricated via a simple two step approach from poly(m-phenylenediamine) micro-spherical shell (PmPDMS). The PmPDA were firstly formed by freeze drying and then crosslinked together via the oxidative polymerization of surface groups in following anneal progress. The PmPDA is hydrophilic before annea progress and become hydrophobic (the contact angle is 103.7°) after it be annealed in air. Moreover, the obtained ultra-flyweight PmPDA (ρ=0.8 mg cm^{-3}) have large surface area (338 m^2 g^{-1}), low thermal conductivity (0.0125 W m^{-1} K^{-1} at 25 ˚C) and excellent mechanical properties. Finally, the regenerated aerogels keep its original shape and ultrahigh absorption capability after more than 10 cycles, making the PmPDA ideal candidates for practical applications in absorption-removal of organics, particularly in the environmental protection and pollution control.

1. Introduction

Since the found of aerogels by Kistler in 1930s [1], it have attracted researchers's great attention due to their high porosity, large surface area, electrical conductivity, high water absorptivity, good elasticity, and extremely low bulk density [2-6]. The traditional aerogels have been mainly focused on silica aerogels [7] which have been utilized or under investigation for various applications, such as thermal insulation, adsorption, nuclear waste storage, electrochemical energy storage, cosmic dust collectors and catalysis [8-12]. Prakash *et al.* described a means of preparing the silica aerogel films by a simple dipcoating method at ambient pressure without the need for supercritical extraction. It is note-worthy that they add surface groups to the inorganic gel which make drying shrinkage reversible. And they can also generate the silica aerogel films with 98.5% porosity with this approach [13]. However, the preparation of silica aerogel process is complex [14], which limit its application in numerous fields. On the other hand, with the research of carbon material [15-17] which is becoming more and more concern, carbon aerogel [15, 17] materials have been widely research. One of the most representative is the graphene aerogels [7, 18-22]. Gao *et al.* [15] synthesized carbon aerogel by freeze-drying aqueous solutions of carbon nanotube and giant graphene oxide (GGO) sheets followed by chemical reduction of GGO into graphene with hydrazine vapor. The carbon aerogel has high elasticity, compression experiments on it showed a nearly complete recovery after 50–82% compression. What's more, it possesses super-high absorption capacities and ultrafast absorption rate for organic solvents and oils. In addition, it is ultra-flyweight aerogel with a density less than 1 mg cm^{-3}, which is even smaller than nitrogen. And the carbon aerogel is also the lightest aerogels in the world. It is noteworthy that it can be easily manufactured in a large-scale due to its tunable size. However, the π-π stacking interactions between graphene sheets can result in the unsuccessful construction of three-dimensional graphene aerogels structures [23]. In addition, the potential for obtaining large quantities of graphene by a low-cost production process is difficult [24]. Due to the production process complicated, which limit its application in the carbon aerogel fields.

On the other hand, conducting polymers such as: polyaniline (PANI), polythiophene (PTH), polyparaphenylene (PPP), polypyridine (PPY) and polyaniline derivatives (such as: poly(o-phenylenediamine) (PoPD), poly(p-phenylenediamine) (PpPD) and poly(m-phenylenediamine) (PmPD)) have been the subject of considerable attention concerning their applications in catalysis, optoelectronic materials, fuel cell, fluorescent probes, sensors, organic batteries, diodes, and unique electrical, optical and photoelectric properties [25-43]. Among numerous conducting polymers, PANI has attracted persistent attention owing to its low cost, environmental compatibility, excellent electrical conductivity, large pseudo-capacitance, and fast doping/dedoping rate during charge/discharge proces, which is the most typical conducting polymers [44]. Xuan *et al.* synthesized magnetically responsive Fe_3O_4@PANI@Au nanocomposites via an ultrasound-assisted in situ surface polymerization method. They also proved the negatively charged Au nanoparticles with a diameter of about 4 nm have been effectively assembled onto the positively charged surface of the as-synthesized Fe_3O_4@polyaniline core/shell microspheres via electrostatic attraction [45]. Sun *et al.* reported on the simple synthesis of submicrometer scale conjugation polymer PoPD colloids by

direct mixing of aqueous PoPD and potassium bichromate solutions at room temperature [45]. Our previous research show the poly(p-phenylenediamine) nanofibers having conjugated structures and can be used as a highly selective fluorescent probe for thiols, L-cysteine and caffeine [25, 31, 32]. We also reveal synthesis of Ag nanoparticles-decorated poly (m-phenylenediamine) hollow spheres and the application for hydrogen peroxide detection [35]. However, to our best knowledge, the synthesis of poly(m-phenylenediamine) aerogel has not been reported clearly.

Here, we report the ultra-flyweight hydrophobic poly(m-phenylenediamine) aerogel (PmPDA) which was fabricated via a simple two step approach from poly(m-phenylenediamine) micro-spherical shell (PmPDMS). The freeze drying-anneal crosslinking progress is easy and lowcost. The PmPDA were firstly formed by freeze drying and then crosslinked together via the oxidative polymerization of surface groups in following anneal progress. It is interesting that the PmPDA is hydrophilic before annea and is hydrophobic after it be annealed in air. The obtained ultra-flyweight (ρ=0.8 mg cm^{-3}) PmPDA have large surface area (BET=338 m^2 g^{-1}) low thermal conductivity (0.0125 W m^{-1} K^{-1} at 25 °C) and excellent mechanical properties. The formation mechanism of PmPDA is demonstrated by X-ray photoelectron spectrum (XPS) results. Furthermore, the PmPDA can be used as a high-performance selectivity adsorbent for oil contamination.

2. Experimental

2.1 Materials

All the chemicals (m-phenylenediamine (mPD), $(NH_4)_2S_2O_8$ (APS), Sudan Red and methylbenzene) were purchased from Aladdin. (Shanghai, China) and used as received without further purification. The water used throughout all experiments was purified through a Millipore system.

2.2 Characterisation

The structure and morphology were investigated by scanning electron microscope (SEM) (FEI Sirion-F250) with an accelerating voltage of 20 kV, transmission electron microscope (TEM) (FEI Tecnai G2 20 STWIN) with an accelerating voltage of 200 kV. Raman spectra were recorded on a Thermo Fisher DXR using an Ar^+ laser (wavelength 532 nm, 2 mW) with 1 μm laser spot equipped with optical microscopy. Fourier transform infrared (FTIR) was performed on a Nicolet 6700 (resolution 0.4 cm^{-1}) infrared spectrometer and samples were dispersed in potassium bromide and compressed into pellets. The XPS was derived from measurements conducted on an X-ray photoelectron spectrometer using an Mg-Kα radiation excitation source (AXIS ULTRA DLD, Kratos). The phase compositions of the as-prepared products were determined by X-ray diffraction analysis (XRD, Rigaku D/max-2500) using graphite-monochromised Cu-Kα radiation. The specific surface area, pore size, and pore volume were determined by a Brunauer-Emmett-Teller (BET) apparatus, V-Sorb 2800P (Gold APP Instruments Corporation, China). The surface area was determined by evaluating the isotherm of the physical adsorption of nitrogen and the specific surface area was determined by the BET method. The surface area of the mesopores was calculated by applying the Battet-Joyner-Halenda adsorption (BJH) approach.

2.3 Synthesis of PmPDMS

The typical preparation process of PmPDMS is as follows: 4.5 g mPD was dissolved in 30 mL deionized water. Then, the mPD solution was cooled in ice-water bath for 2 h in dark condition before oxidative polymerization. Then, 18 mL 1.67 M of APS aqueous solution was added gradually to mPD solution with a magnetic stirrer. After that, the resulting solution was stirred for another 5 min to ensure complete mixing and then the reaction was allowed to proceed without agitation for 24 h at 4 °C. Finally, the product was centrifuged and washed with deionized water till the filtrate became colorless and then dried in a vacuum at 60 °C for 24 h.

2.4 Synthesis of PmPDA

The typical preparation process of PmPDA is as follows: firstly, 4 mg PmPDMS was dispersed in 5 mL deionized water and then the resulting mixture was sonicated for about 10 h to yield a homogenous suspension. Then, the suspension was poured into a cylindrical crucible and freeze-dried for 2 days. The as-prepared PmPDA foam was crosslinked by annealed at 160 °C in air for 24 h, followed by vacuum-drying at 80 °C for 24 h.

3. Results and discussions

3.1 Characterization of PmPDA

Fig. 1 shows the typical SEM and TEM images of PmPDA. Obviously, the PmPDA with porous structure is deposited by homogeneous micro-spherical shell (PmPDMS) with size distribution of 80-120 nm (Figure 1a, b and Figure 2 a). As seen from typical high magnification SEM and TEM images (Figure 1c and d) of a single PmPDMS, the edges of the PmPDMS can be clearly recognised, and the wall thickness if a single particle is about 10 nm. The high surface area and porous structure will be conducive to rapid dye absorption. The electron diffraction data (Figure 1d inset) shows on crystalline structure of PmPDMS which indicates the products are amorphous.

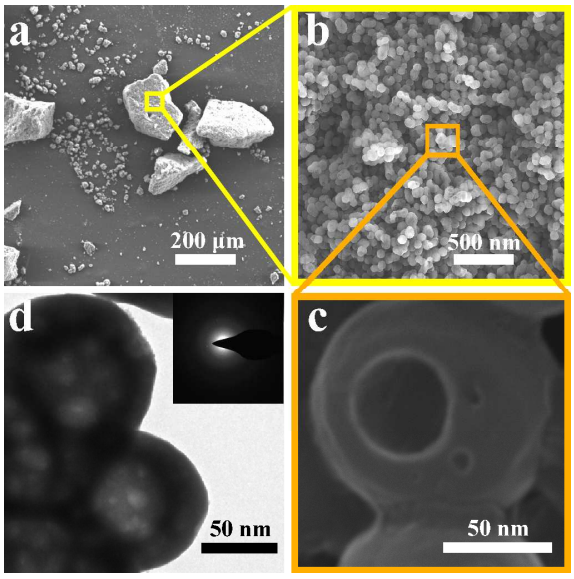

Figure 1 (a, b, c) FESEM images of PmPDA under different magnification, (d) TEM image of PmPDA. Inset: electron diffraction data of PmPDMS in PmPDA.

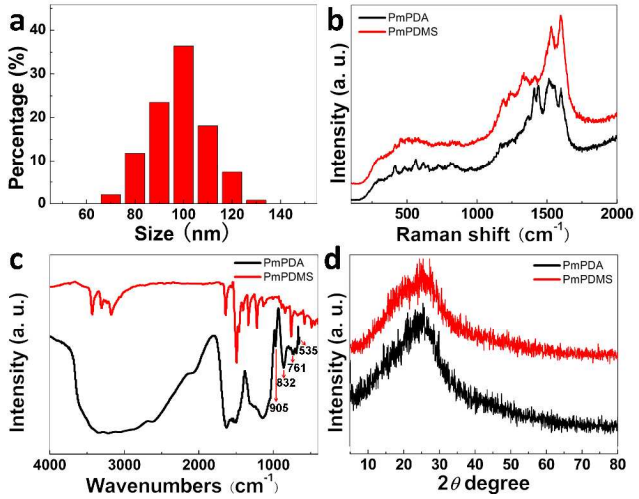

Figure 2 (a) Corresponding size distribution histograms of PmPDMS in PmPDA, (b) Raman spectra of PmPDA and PmPDMS, (c) FTIR spectra and (d) XRD spectrum of PmPDA and PmPDMS.

Raman spectra of PmPDA and PmPDMS are shown in Figure 2b. There are obvious difference in Raman spectra of PmPDA and PmPDMS. The peak at 1170 cm^{-1} is due to the C–H in-plane bending mode, which indicates the presence of quinoid ring. The weak band at 1200 cm-1 is assigned to the C–N stretching mode of polaronic units [36, 38-40]. The peaks located between 1420 and 1370 cm^{-1} are assigned to the C–N+ stretching modes of the delocalized polaronic charge carriers [39]. The peak at 1520, 1549 and 1494 cm^{-1} correspond to the N–H bending deformation mode the C–C deformation of benzenoid rings and quinoid rings, respectively [38]. Moreover, the peak at 1622 cm^{-1} is assigned to the benzene ring [40].

The FT-IR spectrum of PmPDA is shown in Figure 2b. The peaks at 761 and 565 cm^{-1}, characteristic of C-H out-of-plane bending vibrations of benzene nuclei in the phenazine skeleton, respectively [38, 39]. The peaks at 905 and 832 cm^{-1} correspond to the out-of-plane deformation of C–H on a 1, 2, 3, 5-tetrasubstituted benzene ring. The peaks at 1242 and 1371 cm^{-1} are associated with the C–N stretching in the benzenoid and quinoid imine units [37]. The strong peaks at 1600 and 1545 cm^{-1} are assigned to C=N and C=C stretching vibrations in phenazine structure, respectively. Moreover, the peaks at 3325, 3244 and 3206 cm^{-1} correspond to the N–H stretching mode, and imply the presence of secondary amino groups , respectively [43]. The XRD patterns of PmPDA and PmPDMS are shown in Figure 2c. Both PmPDA and PmPDMS show a broad band centered at 2θ = 18–30°, indicat that the PmPDA and PmPDMS are amorphous.

Figure 3a shows the photos of PmPDA cylinder before and after anneal progress. It is clear that before anneal progress, the PmPDA can be easily destroyed (Figure 3b). This indicates the PmPDA has incompact structure before anneal progress. Moreover, it can be wetted easily by water, which illustrates the PmPDA is hydrophilic before anneal progress. In contrast, the PmPDA cylinder shows good mechanical property and can float on the water after anneal progress. This indicates the PmPDA have stable structure and is hydrophobic (the contact angle is 103.7°) after be annealed in air. Moreover, the apparent density of PmPDA is 0.8 mg cm^{-3} which is much smaller than air (1.25 mg cm^{-3}, 25 °C). Figure 3c shows a 5 cm^3 PmPDA cylinder standing on flowers.

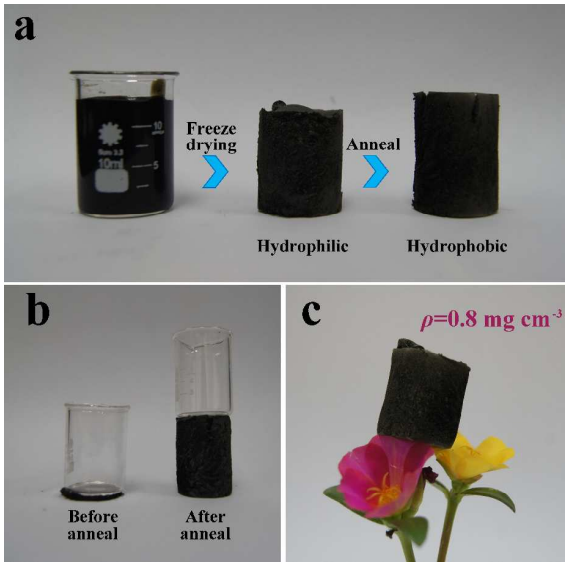

Figure 3 (a) Digital photo of the preparation progress of PMPDA, (b) digital photo of PMPDA under pressure before (left) and after (right) anneal, (c) a 5 cm^3 PMPDA cylinder standing on a flower.

3.2 Formation mechanism of PmPDA

In order to study the formation mechanism of PmPDA, the XPS data of PmPDMS and PmPDA were investigated (Figure 4). Fig. 5a shows the XPS survey spectrum of PmPMS, the N (399 eV) and C (284 eV) can be detected. The N/C atomic ratio is 32.7 % which is close to the monomer (mPD, N/C=33.3%).

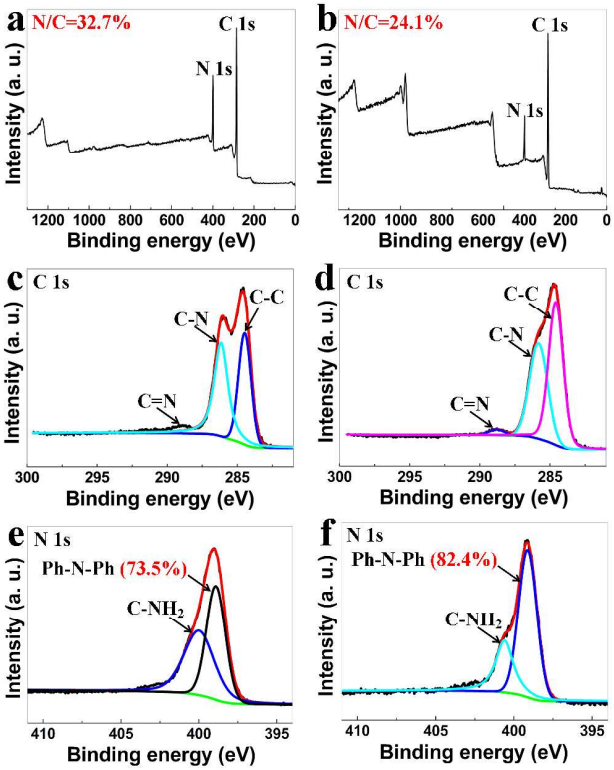

Figure 4 XPS spectra of PMPDA (a) before anneal, (b) after anneal, respectively; C 1s core-level and corresponding deconvoluted spectra for PMPDA (c) before anneal, (d) after anneal, respectively; N 1s core-level

and corresponding deconvoluted spectra for PMPDA (e) before anneal, (f) after anneal, respectively.

The core-level XPS spectrum of C 1s and the corresponding deconvoluted spectra for the PmPDMS are shown in Figure 4c. The peak with a binding energy centered on 284.73 eV could be attributed to the C-C bond. The peaks with binding energies of 286.09 and 288.77 eV can be assigned to the C-N and C=N bonds, respectively [37]. The high-resolution N 1s spectrum (Figure 4e) shows reveals the presence of amidogen N (398.45 eV) and C-N=C (phenothiazine structure, 400.50 eV) [36, 37]. The proportion of amidogen N in total N element is about 36.5%. While for the PmPDA, the intensity of N 1s peak become weak, and the N/C atomic ratio is 24.1 % (Figure 4b), suggesting the loss of N element. The proportion of amidogen N in total N element is about 17.6% Figure 4f) which is much lower than PmPDMS. Reducing of amidogen N indicates the most amidogen N were crosslinked in anneal progress. Moreover, the reducing of amidogen N is also the key factor of the hydrophobicity of this aerogel. There are lots hydrophilic groups (mostly are amido) in PmPDMS before the anneal progress, the products have good hydrophilicity. However, most amidogen N were crosslinked after anneal progress. The PmPDA is hydrophobic and can easily floating on the water.

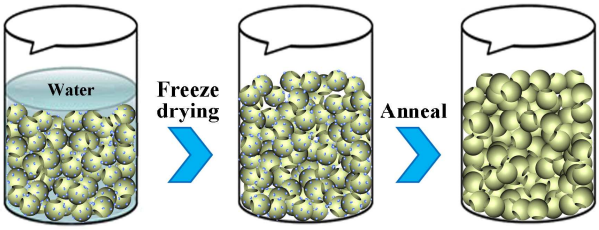

Figure 5 A schematic diagram of morphology forming mechanism. The blue ball represents the surface groups in PmPDMS.

Thus, the formation mechanism of PmPDA is shown in Figure 5 and as follows: firstly, the hydrophilic PmPDMS with incompact structure formed special shape via freeze drying progress. The PmPDMS piled up and there are no chemical bonds between these particles. Furthermore, the PmPDMS have interactive surface groups (amido) at the surface. Subsequently, the PmPDMS crosslinked together via the oxidative polymerization of surface groups in anneal progress. The obtained hydrophilicity PmPDA with good mechanical properties was formed.

3.3 Mechanical properties and absorption of oil contamination

The obtained PmPDA is ultra-flyweight and have excellent mechanical properties. The apparent density of PmPDA is 0.8 mg cm^{-3} which is much smaller than air (1.25 mg cm^{-3}, 25 □). The low density of PmPDA indicates that the PmPDA have large surface area. Figure 6 shows the N_2 adsorption/desorption isotherms and corresponding pore size distribution curve for PmPDA. The isotherms exhibited the characteristics of type IV isotherms with a hysteresis loop (Figure 6a) [46]. It can be seen that the isotherms showed little uptake at low relative pressures (P/P_0 < 0.1), indicating the existence of micropores. Significant hysteresis of the isotherms at high relative pressures (P/P_0 > 0.1) can be seen which indicated that PmPDA was rich in mesopores. Moreover, there was an upward trend at high relative pressures (P/P_0 > 0.90), which may have originated from the presence of macropores. The PmPDA exhibited a highly-developed, hierarchical porosity framework of micropores together with macropores and mesopores, which matched SEM observations (Figure 6a). The pore size distribution data for the aerogel ranged from 2 to 800 nm (Figure 6b), and the size of most of the pores being between 2 to 15 nm. The average pore size was 3.21 nm. The specific surface area was determined, by use of the BET model, to be 338 m^2/g, whereas the pore volume, determined from the BJH model, was 0.72 cm^3/g.

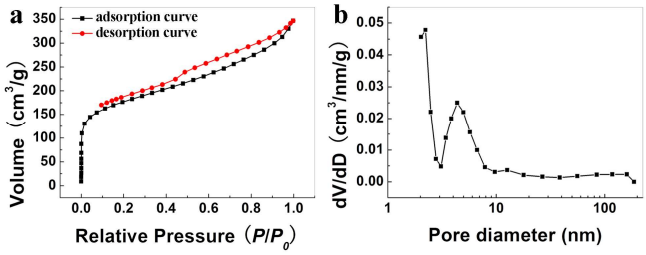

Figure 6 (a) N_2 adsorption/desorption curve and (b) Pore size distribution based on the BJH model of the PMPDA.

This obtained aerogel also have good mechanical properties: 4 mg of PmPDA cylinder could support a static load of at least 100 g and exhibited good resilience when released from compression. As shown in Figure 7a-c, when the compression was released, the sample almost recovered its original shape, indicating the sample was strong and resilient. Moreover, the PmPDA can be used as a spring which have good recovery performance. Figure 7d shows the height change of PmPDA cylinder under 50 compressing cycles. It is clear that there is no significant change in height of PmPDA cylinder even after it is compress for 50 times.

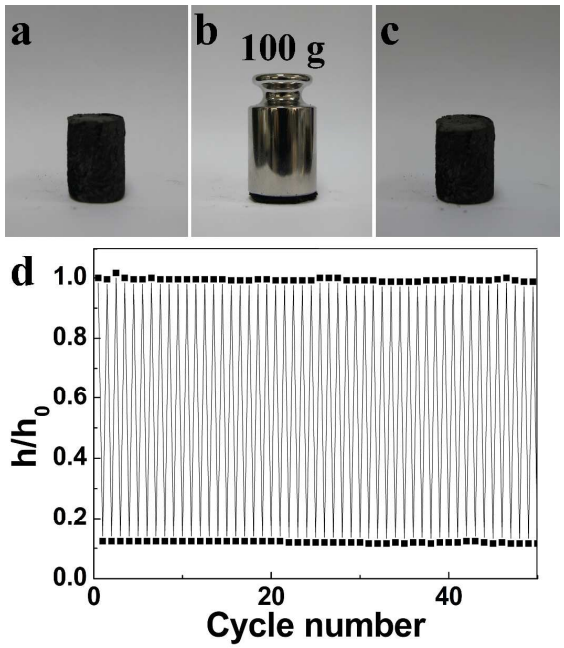

Figure 7 (a-c) Digital photos of PMPDA under 100 g added mass, (d) height change of PmPDA cylinder under 50 compressing cycles.

The good mechanical properties and large surface area of ultra-flyweight hydrophilicity PmPDA indicate this aerogel indicates it posses high absorption capacities and ultrafast absorption rate for

organic solvents and oils. As shown in Figure 8a-d, 0.5 g methylbenzene (stained with Sudan Red) on water is absorbed completely by a 4 mg PmPDA within 5 s, indicating an average absorption rate of 25 g g^{-1} s^{-1}. The high absorption capacities and adsorption rate is remarkable. The PmPDA have good regioselective for organics which can be easily ignited after the adsorption process (Figure 8e, Viedo 1 in supporting information) due to the hydrophobicity of PmPDA. Moreover, this aerogel can be easily picked up by hand after burning (see Viedo 1 in supporting information) indicates the PmPDA have low thermal conductivity. The low thermal conductivity (0.0125 W m^{-1} K^{-1} at 25 ˚C) can be attributed to the three-dimensional porous structure of PmPDA.

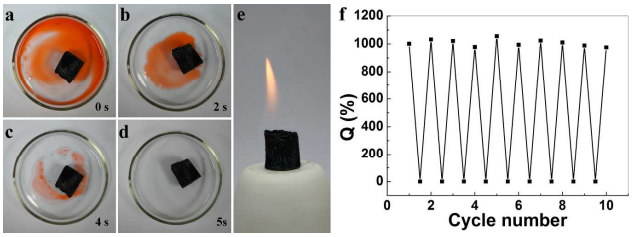

Figure 8 Digital photos of absorption process of toluene (stained with Sudan Black B) on water by the PmPDA within 5 s, (a) 0 s, (b) 2 s (c) 4 s, (d) 5 s; (e) digital photos of ignited PmPDA after absorption process. (f) The restored weight of PmPDA after removing the methylbenzene be completely burned off from the aerogels.

Table 1 shows the absorption capacities (Q is the ratio of the final weight after full absorption to the initial weight of PmPDA) of the PmPDA to various solvents and oils. The absorption capacities 837–1986 g g^{-1} to various solvents. The large absorption capacities indicate this aerogel have excellent adsorption capacity.

Table 1 Absorption capacities (Q is the ratio of the final weight after full absorption to the initial weight of PmPDA) of the PmPDA to various solvents and oils.

solvents	Q/%
methylbenzene	1002
benzene	968
CCl_4	1986
$CHCl_3$	1769
diethyl ether	894
n-hexane	837
cyclohexane	951
ethyl acetate	1139
nitrobenzene	1420
chlorobenzene	1288

Moreover, due to the fine elasticity and low thermal conductivity of PmPDA, the absorbed liquids can be completely burned off from the aerogels in air without destroying the porous structures. The regenerated aerogels still keep the original shape and ultrahigh absorption capability after more than 10 cycles (Figure 8f), making the PmPDA ideal candidates for practical applications in absorption-removal of organics, particularly in the environmental protection and pollution control.

4. Conclusions

In summary, the ultra-flyweight hydrophobic PmPDA was fabricated via a simple two step approach from PmPDMS. The PmPDA were firstly formed by freeze drying and then crosslinked together via the oxidative polymerization of surface groups in following anneal progress. The obtained PmPDA have large surface area (338 m^2 g^{-1}) , low thermal conductivity (0.0125 W m^{-1} K^{-1} at 25 ˚C) and excellent mechanical properties which the density is smaller than air (ρ=0.8 mg cm^{-3}). The formation mechanism of PmPDA and the switch of hydrophilic to hydrophobic is clearly demonstrated by XPS. Moreover, the PmPDA can be used as a high-performance selectivity adsorbent for oil contamination. These findings is helpful for the fabrication of polymer based aerogels and provide insight into the potential use of polymer based aerogels.

Notes and references

[a] *Chemical Synthesis and Pollution Control Key Laboratory of Sichuan Province, College of Chemistry and Chemical Engineering, China West Normal University, Nanchong 637002, P. R. China*
[b] *State Key Laboratory of Functional Materials for Informatics, Shanghai Institute of Microsystem and Information Technology, Chinese Academy of Science, Shanghai 20050, P. R. China*
†*These authors are co-first authors*
**Corresponding author:*
Prof. Liao Fang, Chemical Synthesis and Pollution Control Key Laboratory of Sichuan Province, College of Chemistry and Chemical Engineering, China West Normal University, Nanchong 637002, P. R. China, Tel/Fax: +86 817 2568067, E-mail: liaozhang2003@163.com
Dr. Siwei Yang, State Key Laboratory of Functional Materials for Informatics, Shanghai Institute of Microsystem and Information Technology, Chinese Academy of Science, Shanghai 20050, P. R. China, Tel/Fax: +86 021 62511070 420, E-mail: yangsiwei@mail.sim.ac.cn
‡ This work was supported by China West Normal University Fund (12B017) and China West Normal University Students Research Fund (42713070).

References

1 S. S. Kistler, *Nature*, 1931, **127**, 74.
2 H. Hu, Z. B. Zhao, W. B. Wan, J. S. Qiu, Mater. Interfaces, 2014, **6**, 3242.
3 X. L. Wu, T.Wen, H. L. Guo, S. B. Yang, X. K. Wang, A. W. Xu, *Nano.*, 2013, **4**, 3589.
4 A. C. Pierre, G. M. Pajonk, *Chem. Rev.*, 2002, **102**, 4243.
5 J. Z. Feng, C. R. Zhang, J. Feng, Y. G. Jiang, N. Zhao, *Mater. Interfaces*, 2011, **3**, 4796.
6 Y. J. Wang, G. H. Zhao, S. N. Chai, H. Y. Zhao, Y. B. Wang, *Mater. Interfaces*, 2013, **5**, 842.
7 Y. R. Lin, G. J. Ehlert, C. Bukowsky, H. A. Sodano, *Mater. Interfaces*, 2011, **3**, 2200.
8 D. Sanli, C. Erkey, *Mater. Interfaces*, 2013, **5**, 11708.
9 R. Baetens, B. P. Jelle, A. Gustavsen, *Energy Build*, 2011, **43**, 761.
10 A. C. Pierre, G. M. Pajonk, *Chem. Rev.*, 2002, **102**, 4243.
11 J. P. Randall, M. A. B. Meador, S. C. Jana, *Mater. Interfaces*, 2011, **3**, 613.
12 M. Tabata, I. Adachi, H. Kawai, T. Sumiyoshi, H. N. I. Yokogawa, Methods Phys. *Res. Sect.*, A 2012, **668**, 64.
13 S. S. Prakash, C. Jeffrey, A. J. Hurd, S. M. Rao, *Nature*, 1995, **374**, 440.
14 G. Hayase, K. Kanamori, K. Abe, H. Yano, A. Maeno, H. Kaji, K. Nakanishi, *Mater. Interfaces*, 2014, **6**, 9466.
15 H. Y. Sun , Z. Xu, C. Gao, *Adv. Mater.*, 2013, **25**, 2554.
16 Z. Y. Sui, Y. Cui, J. H. Zhu, B. H. Han, *Mater. Interfaces*, 2013, **5**, 9172.
17 H. P. Cong, X. C. Ren, P. Wang, S. H. Yu, *Nano*., 2012, 6, 2693.
18 L. Xiao, D. Q. Wu, S. Han, Y. S. Huang, S. Li, M. Z. He, F. Zhang, X. L. Feng, *Mater. Interfaces*, 2013, **5**, 3764.
19 Z. S. Wu, S. B. Yang, Y. Sun, K. Parvez, X. L. Feng, K. Müllen, *J. Am. Chem. Soc*. 2012, **134**, 9082.

20 M. A. Worsley, P. J. Pauzauskie, T. Y. Olson, J. Biener, J. H. Satcher, T. F. Baumann, *J. Am. Chem. Soc*. 2010, **132**, 14067.

21 G. Rother, L. Vlcek, M. S. Gruszkiewicz, A. A. Chialvo, L. M. Anovitz, L. Bañuelos, D. Wallacher, N. Grimm, D. R. Cole, *J. Phys. Chem. C*, 2014, **4**, 546.

22 G. Rother, E. G. Krukowski, D. Wallacher, N. Grimm, R. J. Bodnar, D. R. Cole, *J. Phys. Chem. C*, 2012, **116**, 91.

23 C. Y. Hou, Q. H. Zhang , Y. G. Li , H. Z. Wang, *Carbon*, 2012, **50**, 1959.

24 S. H. Lee, H. W. Kim, J. O. Hwang, W. J. Lee, J. Kwon, C. W. Bielawski, R S. Ruoff, S. O. Kim, *Angew. Chem. Int. Ed.*, 2010, **49**, 10084.

25 T. T. Zhang, S. W. Yang, J. Sun, X. B. Li, L. He, S. Yan, X. Y. Kang, C. S. Hu, F. Liao, *Synth. Met.*, 2013, **181**, 86.

26 S. W. Yang, D. Liu, F. Liao, T. T. Guo, Z. P. Wu, T. T. Zhang, *Synth. Met.*, 2012, **162**, 2329.

27 S.W. Yang, F. Liao, *Nano*, 2011, **6**, 597.

28 P. Xiong, H. J. Huang, X.Wang, *J. Power Sources*, 2014, **245**, 938.

29 A. Madhankumar, N. Rajendran, *Prog. Org. Coat.*, 2013, **76**, 1445.

30 Z. F. Wang, F. Liao, S. W. Yang, T. T. Guo, *Mat. Lett.*, 2012, **67**, 121.

31 S. W. Yang, F. Liao, *Synth. Met.*, 2012, **162**, 1343.

32 S. W. Yang, S. Q. S. Huang, D. Liu, F. Liao, *Synth. Met.*, 2012, **162**, 2228.

33 X. Wang, H. D. Li, P. Liu, *Electrochim. Acta*, 2014, **125**, 630.

34 F. Liao, S. W. Yang, X. B. Li, S. Yan, C. S. Hu, L. He, X. Y. Kang, X. Song, T. Y. Ren, *Synth. Met.*, 2014, **190**, 79.

35 Z, P, Wu, S. W. Yang, Z. Chen, T. T. Zhang, T. T. Guo, Z. F. Wang, F. Liao, *Electrochim. Acta*, 2013, **98**, 104.

36 T. T. Guo, F. Liao, Z. F. Wang, S. W. Yang, *J. Mater. Res.*, 2012, **3**, 25.

37 S. Yang, J. Sun, X. Li, W. Zhou, Z. Wang, P. He, G. Ding, X. Xie, Z. Kang, M. Jiang, *J. Mater. Chem. A*, 2014, **2**, 8660.

38 U. Olgun, M. Gulfen, *Reactive & Functional Polymers*, 2014, **77**, 23.

39 F. Liao, S. W. Yang, X. B. Li, L. Yang, Z. Xie, C. S. Hu, S. Yan, T. Y. Ren, Z. Liu, *Synth. Met.*, 2014, **189**,126.

40 F. Liao, S. W. Yang, X. B. Li, S. Yan, C. S. Hu, L. He, X. Y. Kang, X. Song, T. Y. Ren, *Synth. Met.*, 2014, **190**, 79.

41 X. F. Wang, Y. H. Shen, A. J. Xie, L. G. Qiu, S. K. Li ,Y. Wang, *J. Mater. Chem.*, 2011, **21**, 9641.

42 S. W. Yang, C. S. Hu, D. Liu, T. T. Zhang, T. T. Guo, F. Liao, *J. Cluster Sci.*, 2014, **25**, 337.

43 F. Liao, S .W. Yang, X. B. Li, L. Yang, Z. Xie, C. S. Hu, L. He, X. Y. Kang, X. Song, T. Y. Ren, *Synth. Met.*, 2014, **189**, 135.

44 S. H. Xuan, Y. X. J. Wang, J. J. C. Yu , K. C. F. Leung, *Langmuir*, 2009, **25**, 11835.

45 J. Tian, H. Li, Y. Luo, L. Wang, Y. Zhang, X. P. Sun, *Langmuir*, 2010, **27**, 874.

46 X. B. Li, S. W. Yang, J. Sun, P. He, X. G. Xu, G. Q. Ding, *Carbon*, 2014, **78**, 38.